



**HAL**  
open science

# Porous structure optimisation of flash-calcined metakaolin/fly ash geopolymer foam concrete

Gabriel Samson, Martin Cyr

## ► To cite this version:

Gabriel Samson, Martin Cyr. Porous structure optimisation of flash-calcined metakaolin/fly ash geopolymer foam concrete. *European Journal of Environmental and Civil Engineering*, 2017, pp.1 - 17. 10.1080/19648189.2017.1304285 . hal-01756702v1

**HAL Id: hal-01756702**

**<https://hal.science/hal-01756702v1>**

Submitted on 2 Apr 2018 (v1), last revised 12 Jun 2019 (v2)

**HAL** is a multi-disciplinary open access archive for the deposit and dissemination of scientific research documents, whether they are published or not. The documents may come from teaching and research institutions in France or abroad, or from public or private research centers.

L'archive ouverte pluridisciplinaire **HAL**, est destinée au dépôt et à la diffusion de documents scientifiques de niveau recherche, publiés ou non, émanant des établissements d'enseignement et de recherche français ou étrangers, des laboratoires publics ou privés.

# **Porous structure optimization of flash-calcined metakaolin / fly ash geopolymer foam concrete**

Gabriel Samson<sup>1</sup>, Martin Cyr<sup>1</sup>

<sup>1</sup> LMDC, INSAT/UPS Génie Civil, 135 Avenue de Rangueil, 31077 Toulouse cedex 04 France.

April 2017

European Journal of Environmental and Civil Engineering

DOI: 10.1080/19648189.2017.1304285

## **Abstract**

This study reports the production and characterization of geopolymer foam concrete (GFC). This material is foreseen for use as a self-bearing insulation material. In order to identify an optimal paste composition, eight mixtures were made and are presented in a ternary diagram (dry extract of alkaline solution, flash-calcined metakaolin (MK) and fly ash (FA)). The characterization of these pastes (initial setting time (IST), shrinkage and compressive strength) indicated an optimal composition corresponding to 25% of activator, 62.5% of MK and 12.5% of FA. The GFCs were then produced by inserting variable amounts of H<sub>2</sub>O<sub>2</sub> (1, 1.5 and 2%) into the geopolymer paste. The fresh GFC porous structure was stabilized with surfactant. The GFCs produced had low densities ( $225 < \rho < 506 \text{ kg/m}^3$ ) associated with low thermal conductivities ( $0.07 < \lambda < 0.12 \text{ W/(m.K)}$ ) and acceptable compressive strength ( $0.5 < R_c < 1.85 \text{ MPa}$ , for samples cured at 20°C). A significant influence of the surfactant content on the porous structure was demonstrated. The lower surfactant content led to a porous structure made of larger bubbles separated by wider matrix walls promoting GFC compressive strength.

**Keywords:** Geopolymer foam concrete (GFC), metakaolin (MK), fly ash (FA), compressive strength, thermal conductivity, porous structure

## 1 Introduction

Considering the energy crisis, it is essential to reduce the environmental footprint of the building sector as it represents around 40% of the global energy demand (in Europe) (Pacheco-Torgal, Faria, & Jalali, 2012; Perez Fernandez, 2008). To achieve this important goal, two levers can be activated: (1) a reduction of the environmental footprint of the materials employed in building applications, (2) an improvement in building thermal efficiency. Heating and cooling represent 60% of building energy demand, a fact that highlights the huge energy savings that would be possible if the thermal insulation of buildings could be improved (Kaynakli, 2012). Building envelopes usually consist of multilayer materials. Some materials are used to ensure bearing properties (concrete wall or blocks) and low conductivity materials are added to ensure thermal insulation. However, during recent decades, foam concrete (FC) has appeared as a serious alternative to classical multilayer envelopes as these materials can have both self-bearing and thermal insulation properties (Samson, Phelipot-Mardelé, & Lanos, 2016a). FCs are often referred to as aerated concrete. These materials offer an interesting compromise between thermal insulation and mechanical ability, and using them facilitates the building construction process. The vast majority of FCs are produced with ordinary Portland cement (OPC) alone or with additions (Ramamurthy, Kunhanandan Nambiar, & Indu Siva Ranjani, 2009). However, OPC is responsible for approximately 7-8% of worldwide CO<sub>2</sub> gas emissions, so the goal of the present work was to find an alternative binder that could be used to produce FC with good thermomechanical properties.

Geopolymer materials are increasingly studied in the recent literature. These materials appear to provide an effective alternative to OPC cement (Pacheco-Torgal, Abdollahnejad, Camões, Jamshidi, & Ding, 2012) because most of them are produced with industrial by-products. Geopolymers are not intrinsically or fundamentally 'low-CO<sub>2</sub>'. However, if mix design and raw materials selection are carried out with a view towards optimisation of environmental performance, the outcomes can result in very significant savings (Provis, Palomo, & Shi, 2015). Geopolymers are based on precursors that have high silicate, SiO<sub>2</sub> and aluminate, Al<sub>2</sub>O<sub>3</sub>, contents. An alkali-activation is performed by means of a high-pH alkaline silicate solution. Several precursors can be used, the most common being metakaolin (MK) and fly ash (FA). MK is produced by calcination of kaolinite at a lower temperature (around 700°C) than OPC (1450°C), which leads to a lower energy demand. FA is the precursor most commonly used for geopolymer production. FA is an industrial by-product from coal-fired thermal plants. Using this industrial by-product rather than letting it stored in a landfill can prevent pollution problems. Geopolymers exhibit good mechanical properties (P. Duxson et al., 2006) and thermal stability (Peter Duxson,

Provis, Lukey, & van Deventer, 2007). All these reasons explain why they are considered as the third generation binder (P. Duxson et al., 2006).

As geopolymer development is a relatively new field compared to OPC materials, only a few studies on geopolymer foam concrete (GFC) can be found in the literature (Zhang, Provis, Reid, & Wang, 2014). Most of the GFCs have been produced with FA. Sanjayan et al. (2015) produced FA GFCs. Low density value ( $403 \text{ kg/m}^3$ ) was achieved with the higher Al content, which led to the lower compressive strength value (0.9 MPa). Kamseu et al. (2015) prepared GFCs with rice hush ash and volcanic FA with Al powder as blowing agent. The lowest thermal conductivity achieved was  $0.15 \text{ W/(m.K)}$ . Novais et al. (2016) prepared FA GFCs (activated with NaOH) and investigated the influence of the blowing agent on geopolymer kinetics and the rheology of the pastes. Low thermal conductivity was achieved ( $0.08 \text{ W/(m.K)}$ ) for a density of  $440 \text{ kg/m}^3$ . However, the porous structures were heterogeneous because the air bubbles were maintained in the paste only by paste yield stress. Ducman and Korat (2016) compared Al powder and  $\text{H}_2\text{O}_2$  as blowing agent for FA GFC production. Al powder foams had bigger pores than the foams produced with  $\text{H}_2\text{O}_2$ . Adding more blowing agent decreased the number of pore, due to coalescence. Compressive strength values ranged from 2.9 to 9.3 MPa for densities between 610 and  $1000 \text{ kg/m}^3$ . Masi et al. (2014) compared different methods to produce FA geopolymer foams. A surfactant and two blowing agents (Al powder and  $\text{H}_2\text{O}_2$ ) were used. The mix-foaming method employed led to intermediate density GFCs ( $1000\text{-}1200 \text{ kg/m}^3$ ) for compressive strength ranging from 3.6 to 7.2 MPa. Mix-foaming method promoted the formation of very small pores. Gas-foaming method led to lower density ( $< 1000 \text{ kg/m}^3$ ) and lower compressive strength (1.7 to 2.4 MPa). With  $\text{H}_2\text{O}_2$ , wider density range was achieved ( $520 - 1410 \text{ kg/m}^3$ ). The blowing agent concentrations were limited to prevent coalescence. However, pores were not well distributed if the amount of  $\text{H}_2\text{O}_2$  was too high because of bubbles buoyancy. Hlaváček et al. (2015) produced FA GFCs using aluminium powder. With Al powder, the off-gas was quick (2 mins). The samples were cured for 12h at  $80^\circ\text{C}$ . The bubbles were trapped due to the viscosity of the paste. The porous structure was controlled by changing the liquid/solid ratio. Increasing this ratio led to bigger pores. Zhang et al. (2015) prepared GFCs with FA and GGBS activated with a solution of NaOH and an sodium silicate solution. They observed that the best compressive strength was obtained by using 20% GGBS substitution for fly ash. For a constant aqueous foam dosage of 5%, the density was around  $1050 \text{ kg/m}^3$  and compressive strength around 12.6 MPa.

GFCs were also produced with MK. Lassinantti Gualtieri et al. (2015) synthesized GFCs by reacting MK with phosphoric acid and using natural calcite/dolomite as blowing agent. The acidic environment of the fresh paste

provoked chemical decomposition of added carbonates with gas release ( $\text{CO}_2$ ) and consequent foam formation. The conductivities values were very low (from 0.070 to 0.091 W/(m.K)) for the density achieved (from 580 to 730  $\text{kg/m}^3$ ). Palmero et al. (2015) produced MK GFCs with different alkali activators. GFCs were then characterized (density, flexural and compressive strengths, thermal conductivity) and good thermomechanical performances were achieved.

The vast majority of GFCs are produced with the gas-foaming method. The main drawback of GFCs produced with FA is that they have to be thermally cured, as FA presents very low reactivity at ambient temperature. However, high temperature cures lead to increase the cost production and embodied  $\text{CO}_2$ . The alternative binders proposed here had to be produced under ambient conditions (or mild temperatures) so as to be economically and environmentally competitive.

This study aims to develop GFCs based on MK and FA binder activated with a commercial alkaline solution. The association of these two precursors to produce GFC is not common. The blowing agent used is hydrogen peroxide ( $\text{H}_2\text{O}_2$ ). The aim is to produce lightweight GFC ( $\rho < 600 \text{ kg/m}^3$ ) to achieve low thermal conductivity ( $\lambda < 0.12 \text{ W/(m.K)}$ ). To be used as self-bearing material, a minimum compressive strength of 1 MPa is needed, so the first step is to identify an optimized mix between MK, FA and the alkaline solution content. The optimized mix is then used to produce GFC. The influences of two main parameters ( $\text{H}_2\text{O}_2$  and surfactant contents) on GFC properties (porous structure, thermal conductivity and compressive strength) are investigated. The influence of three thermal cures on GFC properties is also studied.

## **2 Materials**

### **2.1 Precursors**

FA is composed of fine, spherical, mostly glassy particles (Kutchko & Kim, 2006) principally containing  $\text{SiO}_2$  and  $\text{Al}_2\text{O}_3$ . At ambient temperature, FA reactivity with alkaline solution is very low, which explains why the majority of FA geopolymers are thermally cured (usually between 40 and 90°C). French FA (Silicoline®) coming from coal-fired power plants was used in this study. It was certified as complying with the EN 450-1 standard. The mineral composition is given in Table 1. The amorphous phases  $\text{SiO}_2$  and  $\text{Al}_2\text{O}_3$  make up 37.4 and 13.9% of the product, respectively (XRD and Rietveld analyses).

Flash-calcined MK is composed of plate-like particles that can cause rheological problems. French MK (Argéco Développement®) was used in this study. It is obtained by kaolinite flash calcination at around 700°C. XRD and

Rietveld analyses performed by Pouhet (2015) give the different oxide contents (Table 1). The amorphous phases SiO<sub>2</sub> and Al<sub>2</sub>O<sub>3</sub> make up 29% and 24%, respectively, of this MK (Table 1).

**Table 1. Raw material chemical composition.**

		SiO <sub>2</sub>	Al <sub>2</sub> O <sub>3</sub>	CaO	MgO	Fe <sub>2</sub> O <sub>3</sub>	K <sub>2</sub> O	Na <sub>2</sub> O	TiO <sub>2</sub>	SO <sub>3</sub>	H <sub>2</sub> O	Loss on ignition	Amorphous phase			
													SiO <sub>2</sub>	Al <sub>2</sub> O <sub>3</sub>	SiO <sub>2</sub> / Al <sub>2</sub> O <sub>3</sub>	SiO <sub>2</sub> / Na <sub>2</sub> O
MK	%	68.1	24.1	0.2	0.2	3.7	0.4	0.1	1.1	0.0	-	1.8	29.0	24.0	2.1	878.0
FA	%	49.7	26.3	1.7	1.6	6.0	4.2	0.6	0.8	-	-	2.5	37.4	13.9	4.5	85.4
Bétol 47T	%	27.5	-	-	-	-	-	16.9	-	-	55.6	-	-	-	-	1.7

## 2.2 Alkaline solution, blowing agent and surfactant

A commercial sodium silicate solution (Bétol 47T - Woellner®) was used to activate the precursors. Its chemical composition is given in Table 1. The activation was enhanced by a small addition of caustic soda (3.2% of the mass of the commercial alkaline solution). The material of the alkaline solution remaining after water evaporation is referred to as the activator (44.4%). Hydrogen peroxide H<sub>2</sub>O<sub>2</sub> (purity 50% - Solvay) was used as the blowing agent. Gas-voids were created throughout the fresh paste when the H<sub>2</sub>O<sub>2</sub> was transformed into O<sub>2</sub>. A commercial surfactant was employed to stabilize the GFC porous structure before the geopolymer paste set. Binder densities and specific surface (Blaine value) were provided by the precursor producers (Table 2). The particle size distributions were established with a Cilas 1090 LD LASER granulometer (Figure 1).

**Table 2. Raw material physical characteristics, \* = obtained with BET analysis (San Nicolas, Cyr, & Escadeillas, 2014).**

	Granulometry					
	Density	Blaine specific surface	d <sub>10</sub>	d <sub>50</sub>	d <sub>90</sub>	d <sub>moy</sub>
	kg/m <sup>3</sup>	cm <sup>2</sup> /g	µm	µm	µm	µm
Measure precision	100	200	0.2	0.2	0.2	0.2
MK	2500	13000*	5.1	28.0	81.9	36.8
FA	2200	2730	6.7	37.7	97.0	37.7

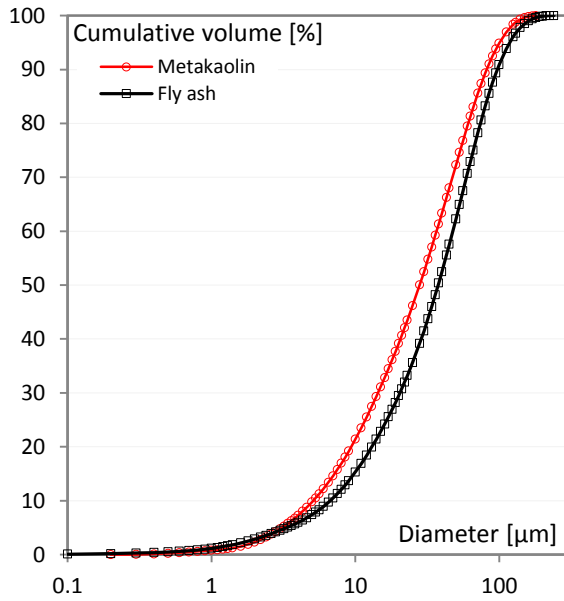


**Figure 1. Precursor particle size distributions.**

### 3 Methods

#### 3.1 Mix-design

Eight mixes (see ternary diagram - Figure 2) were produced and analysed to determine the best proportions of MK, FA and activator. This type of diagram offers the possibility to represent the results (section 4) with colour gradients, which enables to better understand how paste properties evolve according to binder composition. The mix proportions and associated results are presented in Table 3. A ternary diagram was built by changing the proportion of the three raw materials (MK, FA and activator). The different compositions are referred to as  $A_iMK_jFA_k$  where A is the activator and i the associated percentage; j and k are MK and FA percentages, respectively. Each sample verified  $i + j + k = 100$ . FA content was kept lower than or equal to MK content ( $k \leq j$ ).

The same water/binder mass ratio ( $W/B = 0.36$ ) was used for all compositions. The binder comprised the dry powders (MK and FA) and the activator (dry extract of the alkaline activator). The water came from the alkaline solution and a suitable amount of water was added to obtain a constant W/B ratio for each mix. As MK requires more water (Zuhua, Xiao, Huajun, & Yue, 2009), the minimum value of the W/B ratio was evaluated with preliminary tests using the samples that contained only MK ( $A_{25}MK_{75}$  and  $A_{15}MK_{85}$  - Table 3). The minimum W/B ratio was identified as the smallest ratio required for the mixtures to fill all the moulds without vibration. With lower W/B, it becomes very difficult to fill all the moulds without vibration for the pure MK pastes. Two activator percentages (15 and 25%) were employed to assess the influence of the alkaline activator quantity on the properties of the MK-FA blended geopolymers.

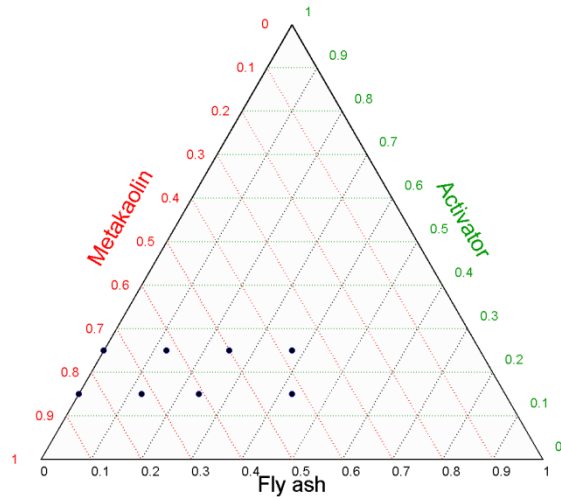


Figure 2. Mix-design: Ternary.

Table 3. Sample compositions and test results.

Unit	Ternary composition			Molar ratio				Initial setting time (IST)	Shrinkage					Compressive strength		
	Activator	MK	FA	SiO <sub>2</sub> /Al <sub>2</sub> O <sub>3</sub>	SiO <sub>2</sub> /Na <sub>2</sub> O	Na <sub>2</sub> O/Al <sub>2</sub> O <sub>3</sub>	H <sub>2</sub> O/Na <sub>2</sub> O	Ts	Δl / l <sub>0</sub>					R <sub>c</sub>		
	%	%	%	-	-	-	-	mins	%					MPa		
Time [days]									2	7	14	21	28	1	7	28
A <sub>25</sub> MK <sub>75</sub>	25.0	75.0	0.0	3.5	3.8	0.9	12.5	360	2.2	2.3	2.3	2.4	2.4	21.4	50.5	53.2
A <sub>15</sub> MK <sub>85</sub>	15.0	85.0	0.0	2.8	5.8	0.5	20.7	265	1.2	1.2	1.2	1.3	1.3	2.5	7.7	10.4
A <sub>25</sub> MK <sub>62.5</sub> FA <sub>12.5</sub>	62.5	12.5	25	3.8	3.9	1.0	12.4	380	2.1	2.2	2.3	2.3	2.3	22.0	52.0	54.2
A <sub>25</sub> MK <sub>50</sub> FA <sub>25</sub>	25.0	50.0	25.0	4.3	4.0	1.1	12.4	550	1.5	2.6	2.7	2.7	2.7	7.8	41.6	46.7
A <sub>25</sub> MK <sub>37.5</sub> FA <sub>37.5</sub>	25.0	37.5	37.5	4.8	4.1	1.2	12.3	750	1.4	3.2	3.3	3.3	3.4	3.7	28.1	30.8
A <sub>15</sub> MK <sub>72.5</sub> FA <sub>12.5</sub>	15.0	72.5	12.5	3.1	5.9	0.5	20.5	260	1.0	1.1	1.1	1.1	1.2	5.6	15.9	17.5
A <sub>15</sub> MK <sub>61</sub> FA <sub>24</sub>	15.0	61.0	24.0	3.4	6.0	0.6	20.3	475	1.1	1.2	1.2	1.2	1.2	1.9	10.1	12.0
A <sub>15</sub> MK <sub>42.5</sub> FA <sub>42.5</sub>	15.0	42.5	42.5	3.9	6.2	0.6	20.0	480	1.2	1.3	1.3	1.3	1.3	1.2	9.3	10.2
A <sub>25</sub> MK <sub>61.5</sub> FA <sub>12.5</sub> OPC <sub>1</sub>	61.5	12.5	25.0	3.9	3.9	1.0	12.4	290	1.4	1.7	1.7	1.8	1.8	27.2	51.1	53.7

### 3.2 Production of blended MK-FA samples

Paste production started with the dry mixing of MK and FA powders. Caustic soda was diluted in the water added. This solution was mixed with the alkaline solution, the resulting liquid was added to the powder, and the constituents were mixed for 1 minute at low speed and then 2 minutes at high speed using an ordinary mortar mixer (Automix 65 - Controls®). The fresh paste was cast in the different moulds. The moulds used for the blended MK-FA production and characterization schedule are presented in

Table 4. Water transfer was prevented by covering the moulds with plastic films. The moulds were stored in a room at 20°C for 24h before unmoulding.

Table 4. Geopolymer paste characterization.

Test	Quantity measured	Moulds	Time [days]
Initial setting time (IST)	min	Truncated conical mould - height 40 mm - diameter 80 mm	0
Compressive strength	MPa	Cubic (8 samples) - width 20 mm	1, 7, 28
Shrinkage	%	Prismatic (3 samples) - 20 x 20 x 160 mm	1, 2, 7, 14, 21, 28



### 3.3 Characterization of blended MK-FA samples

The paste initial setting time (IST) was measured with an automatic Vicat device (Vicatronic®). The IST was calculated as the time elapsing between the initial contact ( $t = 0$ ) of dry powder and alkaline solution and the time when the Vicat needle penetration was 25 mm or less (ASTM C191 - 01 standard, 2006). Cubic and prismatic samples were unmoulded after 24h. Cubic samples were stored in plastic bags to limit water loss. Prismatic samples were kept at 20°C and 50% HR for shrinkage tests, performed by adapting (ASTM C596 - 09e1 standard, 2001). These unrestrained shrinkage conditions were quite harsh for early age geopolymer samples. Prismatic samples (3 per composition) were measured at 1, 2, 7, 14, 21 and 28 days. The shrinkage was defined as  $(l-l_0)/l_0$  where  $l$  is the size of the samples and  $l_0$  is their initial size after unmoulding. Compressive strength was measured at 1, 7 and 28 days on 8 cubic samples (100 kN IGM® press, loading speed 0.5 kN/s).

### 3.4 Blended MK-FA GFC production

The optimized mix found was then used to produce GFC. MK, FA and the surfactant were dry mixed. The solution containing the additional water, the caustic soda and the alkaline solution was added to powders and the same mixing process as presented for the paste was followed. Immediately after paste production, the blowing agent  $H_2O_2$  was added to the geopolymer suspension and additional mixing (30s at slow speed and 30s at high speed) was performed to uniformly disperse the  $H_2O_2$  through the paste. A semi-rigid plastic sheet was placed on the internal surface of the cylindrical moulds ( $\phi = 118$  mm) to facilitate unmoulding. The paste was poured into the moulds. The dioxygen gas was slowly released in the paste over around 180 minutes. During this GFC rising step, GFC volume could be multiplied by up to 4, depending on the  $H_2O_2$  content. After 180 minutes, the moulds were covered with plastic film to prevent water loss. All GFCs were kept in their moulds for 7 days. Three curing conditions were investigated:

- GFC stored at ambient temperature (20°C).
- GFC placed in a climatic chamber at 40°C after 180 minutes. At that moment fresh GFC had reached its final height.
- GFC placed in a climatic chamber at 40°C after 15 minutes (at the beginning of  $O_2$  gas-off).

The GFCs were referred to as  $HP_mS_n$ , where HP is hydrogen peroxide ( $H_2O_2$ ) and  $m$  is its percentage.  $S$  refers to surfactant and  $n$  to its percentage. The different GFC compositions and thermomechanical results are presented in Table 5.

### **3.5 Blended MK-FA GFC characterization**

GFC specimens were unmoulded after 7 days, they were around 200 mm high. The central part was sawed to obtain samples 118 mm high and 118 mm in diameter. Samples were then left in an oven at 40°C for a week to dry them. Dry conditions were necessary for measuring their thermal conductivity. After 7 days, the sample masses were stable. The hot wire method (Neotim®) was used to measure thermal conductivities. The compressive strength was then determined with an IGM® press (100 kN, loading speed 0.2 kN/s).

## **4 Results**

### **4.1 Identification of the optimal paste composition**

The performance of geopolymer paste depends strongly on the molar ratios  $\text{SiO}_2/\text{Al}_2\text{O}_3$ ,  $\text{Na}_2\text{O}/\text{Al}_2\text{O}_3$  and  $\text{H}_2\text{O}/\text{Na}_2\text{O}$ . Mixing the three components of the ternary diagram (Figure 2) led to different molar ratios (Table 4).  $\text{SiO}_2/\text{Al}_2\text{O}_3$  ratios ranged from 2.8 to 4.2. FA contained more silicate than MK, which explains why the  $\text{SiO}_2/\text{Al}_2\text{O}_3$  ratio increased with FA content. The  $\text{Na}_2\text{O}/\text{Al}_2\text{O}_3$  ratio mostly depended on the activator content. The IST results are presented in Figure 3.

The IST values achieved were longer than the time required for the fresh GFC to achieve its final height, 180 minutes. For both activation levels, the IST was minimal when the binder contained only MK. Increasing the FA content significantly increased the IST. The highest IST, of 750 minutes, was obtained with  $\text{A}_{25}\text{MK}_{37.5}\text{FA}_{37.5}$  ( $\text{SiO}_2/\text{Al}_2\text{O}_3 = 4.8$ ). The IST of  $\text{A}_{15}\text{MK}_{42.5}\text{FA}_{42.5}$  was lower (480 mins) because of the lower  $\text{SiO}_2/\text{Al}_2\text{O}_3$  ratio (3.9). The globally high IST obtained for samples containing FA is explained by the low reactivity of FA under ambient conditions. If the IST is too long, the porous structure of the fresh GFC has to be maintained for a long time and coalescence problems may appear. MK-FA binders with excessive FA content do not seem appropriate for GFC production (at ambient temperature).

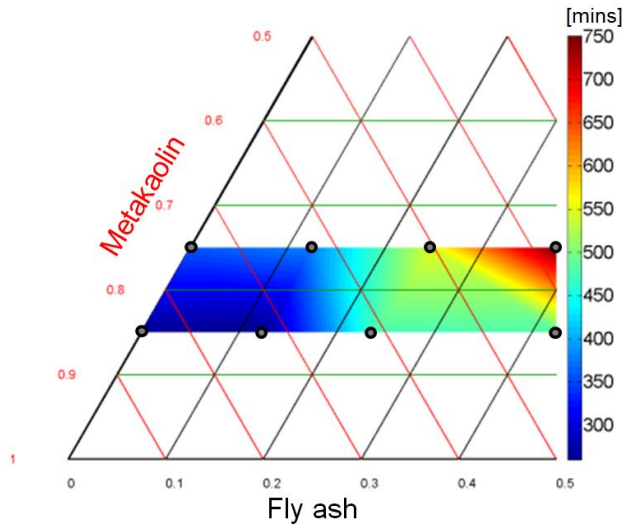


**Figure 3. Initial setting time (IST).**

The shrinkage results are presented in Figure 4. As GFCs present a highly porous structure, they are subject to shrinkage problems. For this reason, shrinkage was first studied on paste to find a matrix presenting relatively low shrinkage that would be suitable for GFC production. Shrinkage was very marked for all compositions (more than 1.2% at 28 days - Figure 4 (c)). Samples were placed in dry conditions (20°C - 50% RH) after only 24 hours. At that time, the geopolymer matrix was far from its final compressive strength and the fast mass loss led to the large shrinkage values observed. At 28 days, the lowest shrinkage values were observed for low activation rate and low FA content (1.3 and 1.2% for  $A_{15}MK_{85}$  and  $A_{15}MK_{72.5}FA_{12.5}$  respectively). For both activation levels, shrinkage increased when FA content became high ( $\geq 24\%$ ). Once again, high FA content was to be avoided (at ambient temperature).

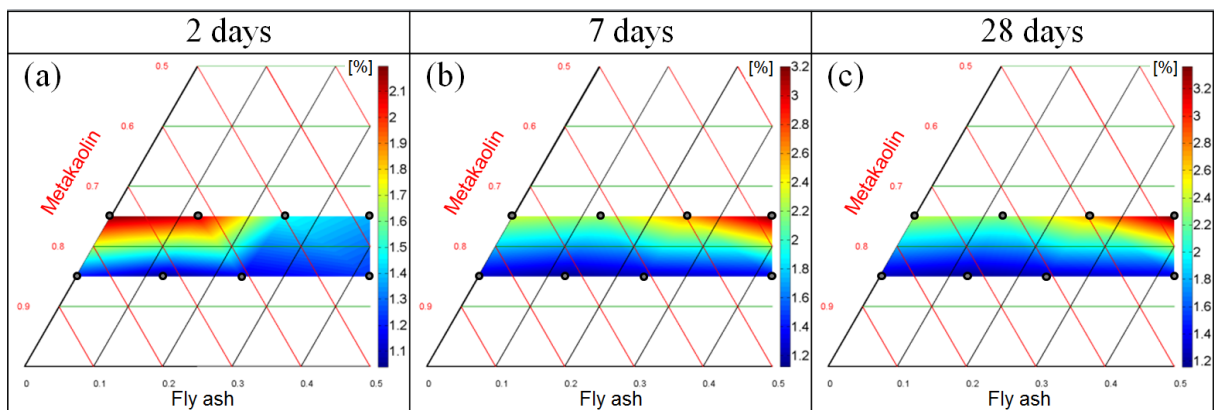


**Figure 4. Shrinkage.**

The evolution of compressive strength is presented in Figure 5. At 1 day, maximum compressive strengths were obtained for high activation levels and reached 22.0 MPa for  $A_{25}MK_{62.5}FA_{12.5}$  (21.4 MPa for  $A_{25}MK_{75}$ ). Higher FA content ( $> 12.5\%$ ) led to a drop in compressive strength ( $Rc_{A_{25}MK_{50}FA_{25}} = 7.8$  MPa and  $Rc_{A_{25}MK_{37.5}FA_{37.5}}$

= 3.6 MPa, at 1 day). Low activation rates could not provide acceptable compressive strength at 1 day whatever the FA content ( $R_c \leq 5.6$  MPa). At 7 days, all compressive strength values had increased. As samples were kept in plastic bags, geopolymerization reactions continued without the apparition of damage due to shrinkage. The highest compressive strength values were again obtained for  $A_{25}MK_{62.5}FA_{12.5}$  and  $A_{25}MK_{75}$  (52.0 and 50.5 MPa respectively). Compressive strengths did not evolve greatly between 7 and 28 days. The highest compressive strength achieved at 28 days was 54.2 MPa ( $A_{25}MK_{62.5}FA_{12.5}$ ).

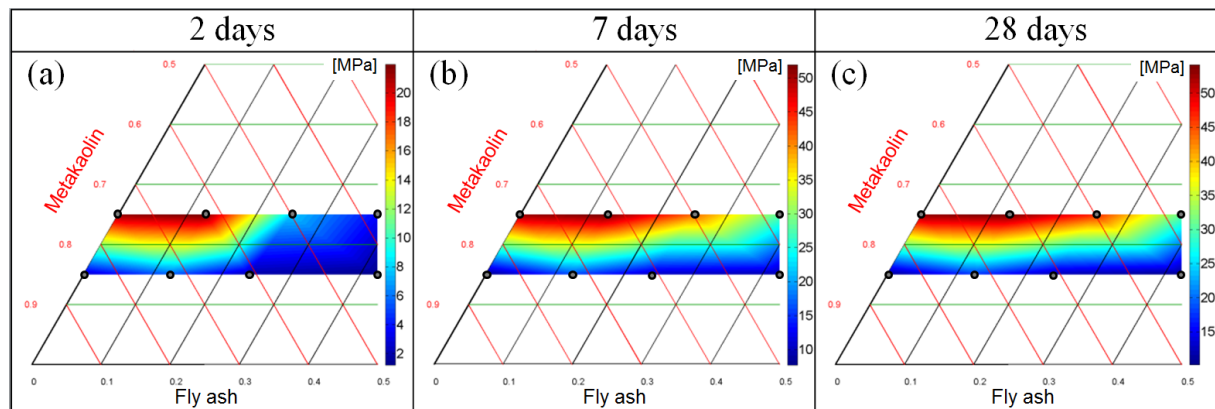


**Figure 5. Compressive strength.**

The best mix for GFC production was selected on the basis of the three parameters studied (IST, shrinkage and compressive strength). GFC compressive strength mostly depends on the matrix strength so the two mixes providing the best compressive strength were chosen ( $A_{25}MK_{75}$  and  $A_{25}MK_{62.5}FA_{12.5}$ ). For  $A_{25}MK_{75}$  and  $A_{25}MK_{62.5}FA_{12.5}$ , ISTs were similar (360 and 380 minutes) and longer than the minimum required time (180 minutes, corresponding to the end of the fresh GFC rising). Therefore, a surfactant had to ensure porous structure stability until the geopolymer matrix had set (around 200 minutes). The 28-day shrinkage values were also similar (2.4 and 2.3 % for  $A_{25}MK_{75}$  and  $A_{25}MK_{62.5}FA_{12.5}$ ). Thus, both mixes presented acceptable properties for GFC production. An additional parameter, the cost, encouraged the selection of  $A_{25}MK_{62.5}FA_{12.5}$ . As MK is more expensive than FA, incorporating 12.5% of FA led to a reduction of the matrix cost.

Lastly, the rather high IST of  $A_{25}MK_{62.5}FA_{12.5}$  could cause problems for GFC porous structure stability until setting, especially if the GFC produced had to simultaneously achieve low density and use a limited amount of surfactant (Samson, Phelipot-Mardelé, & Lanos, 2016b). Reducing matrix IST would also reduce the manufacturing time. For these reasons, 1% of ordinary Portland cement (OPC) CEM I was added in substitution for MK. This significantly decreased the IST (from 380 to 290 minutes) while compressive strength remained

similar (see last line of Table 3). The small OPC addition also had a positive effect on shrinkage. At 28 days,  $A_{25}MK_{62.5}FA_{12.5}$  and  $A_{25}MK_{61.5}FA_{12.5}OPC_1$  shrinkages were 2.3 and 1.8%, respectively.

## 4.2 GFC results

The previous part identified the optimized mix ( $A_{25}MK_{61.5}FA_{12.5}OPC_1$ ), which was then used to produce GFC according to the procedure presented in part 3.4. The influence of two composition parameters ( $H_2O_2$  and surfactant contents) and three curing conditions on GFC thermomechanical properties was investigated.

### 4.2.1 Density

The influence of  $H_2O_2$  content and curing conditions on GFC density is presented in Figure 6. Adding more  $H_2O_2$  led to higher  $O_2$  gas release and lower GFC density, for all curing conditions. For a fixed  $H_2O_2$  content, GFC produced with the higher surfactant content had the lowest density. This indicates that air (entrained air) was already trapped and stabilized on fresh paste because of the quick mixing and the stabilizing action of the surfactant.

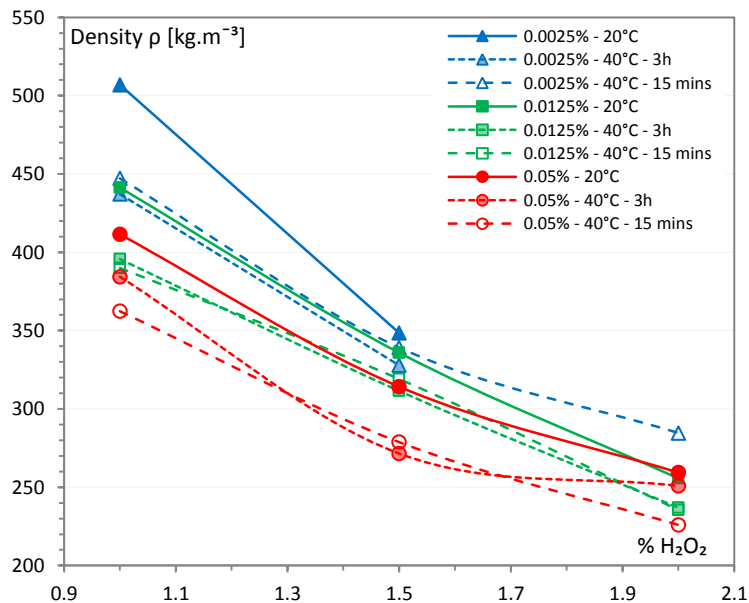


Figure 6. Influence of  $H_2O_2$  content and curing conditions on GFC density.

**Table 5. GFC composition and properties.**

	Curing condition	HP <sub>2</sub> S <sub>0.05</sub>			HP <sub>2</sub> S <sub>0.0125</sub>			HP <sub>2</sub> S <sub>0.0025</sub>			HP <sub>1.5</sub> S <sub>0.05</sub>			HP <sub>1.5</sub> S <sub>0.0125</sub>			HP <sub>1.5</sub> S <sub>0.0025</sub>			HP <sub>1</sub> S <sub>0.05</sub>			HP <sub>1</sub> S <sub>0.0125</sub>			HP <sub>1</sub> S <sub>0.0025</sub>		
		20° C	40° C - 3h	40° C - 15 mins	20° C	40° C - 3h	40° C - 15 mins	20° C	40° C - 3h	40° C - 15 mins	20° C	40° C - 3h	40° C - 15 mins	20° C	40° C - 3h	40° C - 15 mins	20° C	40° C - 3h	40° C - 15 mins	20° C	40° C - 3h	40° C - 15 mins	20° C	40° C - 3h	40° C - 15 mins	20° C	40° C - 3h	40° C - 15 mins
H <sub>2</sub> O <sub>2</sub> content	%	2						1.5						1														
Surfactant content	%	0.05			0.0125			0.0025			0.05			0.0125			0.0025			0.05			0.0125			0.0025		
Density	kg/m <sup>3</sup>	259	251	226	256	237	235	Coalescence			314	272	279	336	311	319	349	328	339	411	384	362	397	396	390	507	437	447
Thermal conductivity λ	W/(m.K)	0.08	0.07	0.07	0.08	0.08	0.07	Coalescence			0.09	0.09	0.08	0.10	0.09	0.09	0.10	0.09	0.09	0.10	0.10	0.10	0.11	0.11	0.10	0.12	0.12	0.11
Compressive strength Rc	MPa	0.49	0.53	0.06	0.48	0.38	0.12	Coalescence			0.70	0.65	0.16	0.88	0.86	0.20	1.03	1.21	0.39	1.07	1.16	0.70	1.04	1.06	0.34	1.85	1.68	1.15

It was not possible to produce a GFC ( $\text{HP}_2\text{S}_{0.0025}$ ) that simultaneously had the lowest surfactant content ( $d = 0.0025\%$ ) and the highest  $\text{H}_2\text{O}_2$  content (2%) for the first two curing conditions. This GFC rose normally to reach its maximum height. However, due to the low surfactant content, the fresh GFC porous structure did not remain stable until the matrix set and uncontrolled coalescence occurred at several points, leading to the collapse of the porous structure. Coalescence appeared when the membrane between two bubbles broke because of insufficient stabilization by the surfactant. Successive coalescences led to big bubbles that escaped from the top of the fresh GFC because of buoyancy force, thus leading to collapse of the GFC. Such collapse indicated that a minimum acceptable surfactant content (depending on  $\text{H}_2\text{O}_2$  content) must exist.

Stable GFCs stored at  $20^\circ\text{C}$  had the highest densities (Figure 6). Very small differences appeared between GFC cured at  $40^\circ\text{C}$  after 15 or 180 minutes. Curing samples at  $40^\circ\text{C}$  must cause mass loss, explaining the lower densities achieved. The small differences observed between ambient temperature and  $40^\circ\text{C}$  curing conditions revealed that, at ambient temperature, more water was chemically bound in the matrix. After 7 days in the moulds, this water was not released by curing. It may have reacted with the OPC to form hydrates or stayed trapped in closed pores of the geopolymer.

#### 4.2.2 GFC thermomechanical performance

The evolution of GFC thermal conductivity is presented in Figure 7 (a). Thermal conductivity mostly depended on GFC density. No significant influence of curing conditions on thermal conductivity could be observed. The GFCs produced exhibited low thermal conductivity ( $\lambda < 0.12\text{ W}/(\text{m}\cdot\text{K})$ ), which means that these materials could be used as thermal insulation materials. In contrast, compressive strength values depended strongly on curing conditions (Figure 7 (b)). Curing a sample at  $40^\circ\text{C}$  after 15 minutes must be avoided as it leads to the lowest compressive strength values. Heating the lateral surfaces of the moulds may have heated the fresh paste samples and reduced the IST of the fresh matrix next to the hot lateral surface, leading to heterogeneity of the porous structure. The third cure ( $40^\circ\text{C}$  at 180 mins) was performed after fresh GFC had reached its final height and was associated with a global increase in compressive strength. The porous structure ceased to evolve after 180 mins, so the compressive strength gain can only be explained by a more solid matrix. As there was some FA in the matrix, it was to be expected that increasing the temperature would activate the FA. Samples conserved at  $20^\circ\text{C}$  had slightly lower compressive strength than samples cured at  $40^\circ\text{C}$  after 180 mins. This can be explained by the fact that FA reactivity was lower at  $20^\circ\text{C}$  than at  $40^\circ\text{C}$ . However, the GFCs exhibited satisfactory compressive strengths regarding the low density achieved, even when they were produced at ambient temperature.

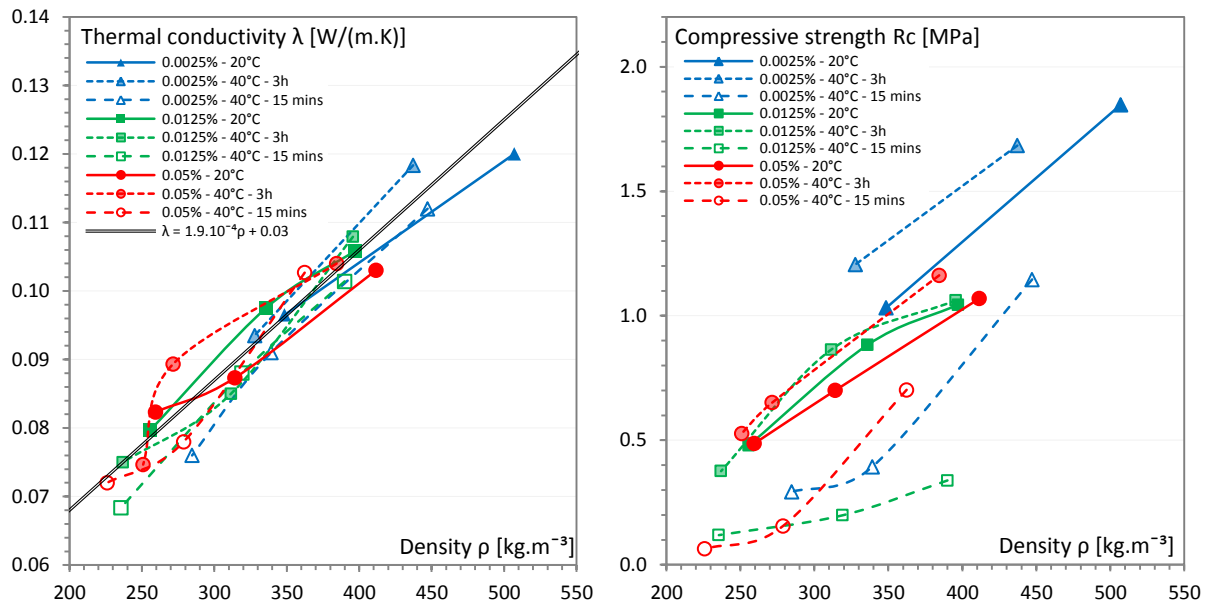


**Figure 7. (a) GFC thermal conductivity; (b) GFC compressive strength.**

Finally, it should be noted that GFC compressive strength also depended on surfactant content. At 20°C, whatever the H<sub>2</sub>O<sub>2</sub> content, low surfactant content was associated with better compressive strength. This was related to the porous structure evolution presented in the next part.

In a recent paper, Samson et al. (2016a) reviewed the thermomechanical properties of FC. They focused on FC made with “classic” binder such as OPC, lime or gypsum. The evolution of FC thermal conductivity depending on density of all these “classic” FCs is presented on Figure 8 (grey squares). Some GFC thermal conductivities are also presented on Figure 8. Thermal conductivity is highly correlated to density for both classic FC and GFCs. The produced GFCs (red squares) present low thermal conductivity in agreement with the low densities reached. The thermomechanical performances of the GFCs cured at 40°C after 15 minutes are not presented because the compressive strength values are small.



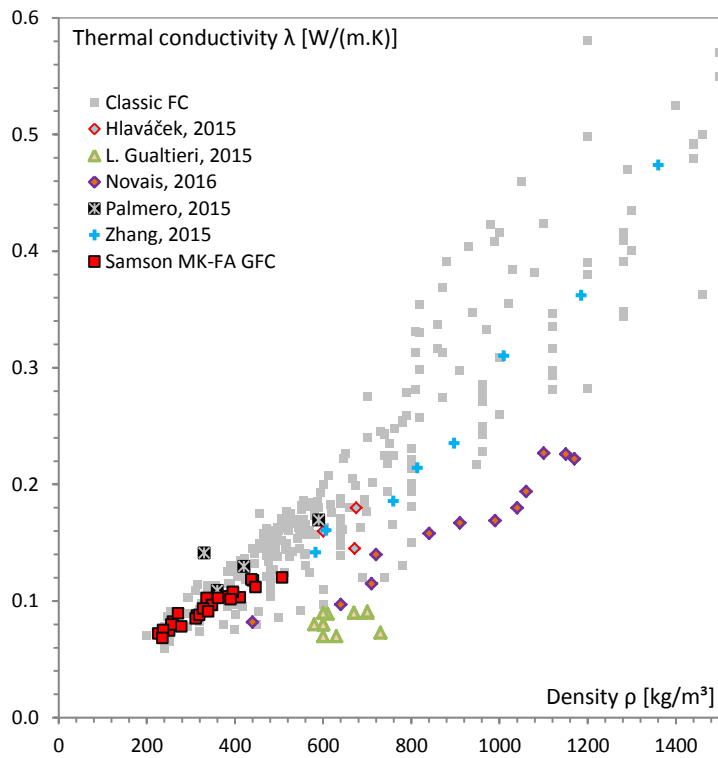


**Figure 8. Comparison of the thermal conductivity values obtained in literature and in this study.**

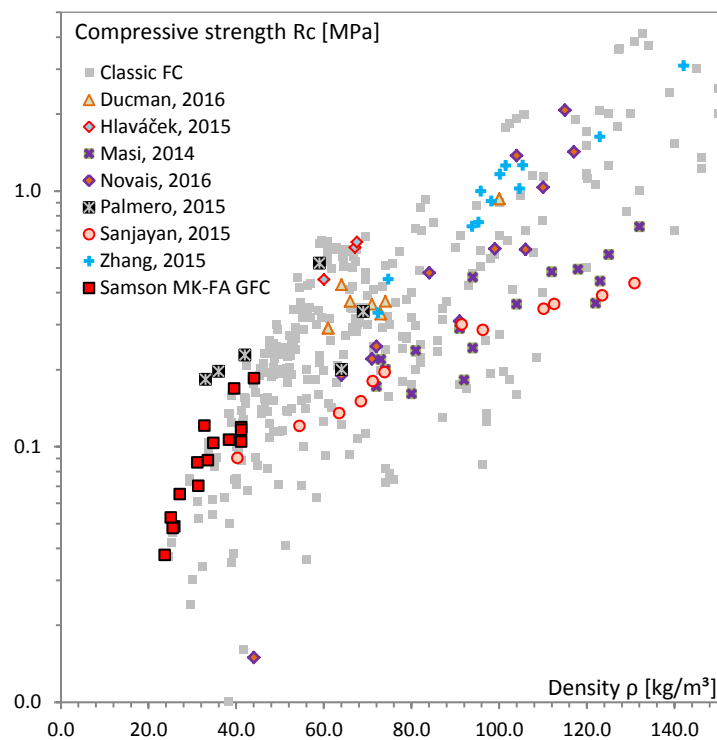


**Figure 9. Comparison of the compressive strength values obtained in literature and in this study.**

Similarly, the compressive strength of the classic FC, GFCs from literature and the produced MK-FA GFCs are presented on Figure 9. Compressive strength values are less correlated to density. Others parameters such as binder type, production process or porous structure lead to bigger compressive strength variations. The MK-FA

GFC produced (red square) exhibit very good compressive strength regarding their low densities. Only one GFC exhibit higher compressive strength (Palmero et al., 2015). Palmero (2015) reach very interesting compressive strength but their samples were cured at high temperature for 24h (65°C). Thus, regarding to compressive strength values, the produced FC present very competitive results regarding to both classic FC and GFCs.

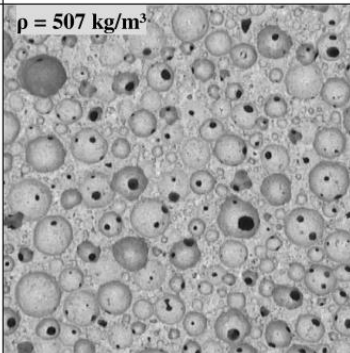
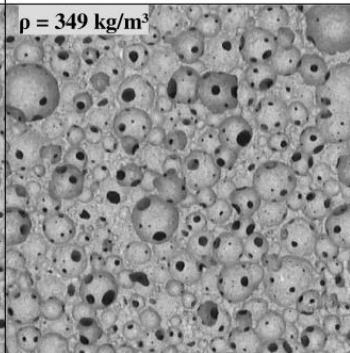
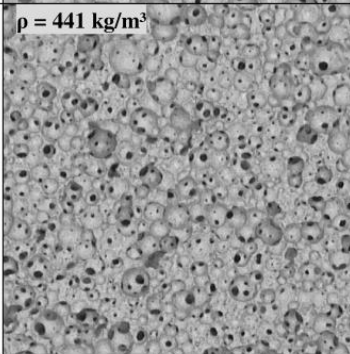
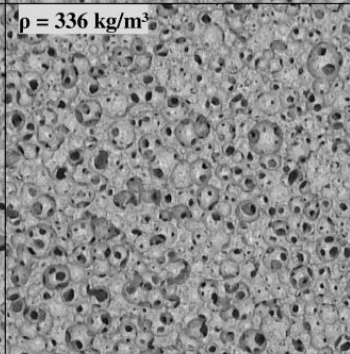
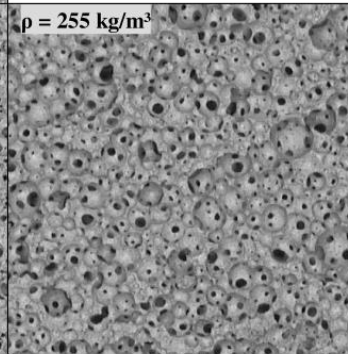
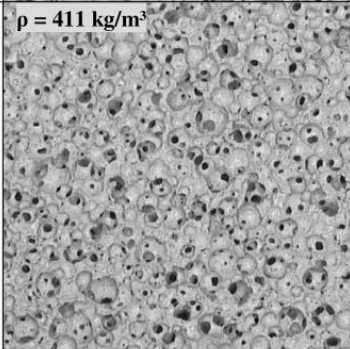
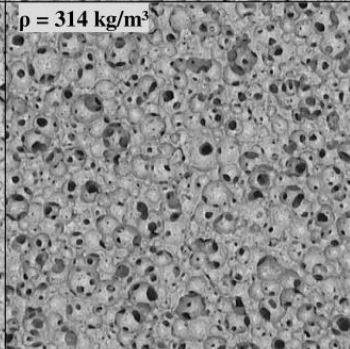
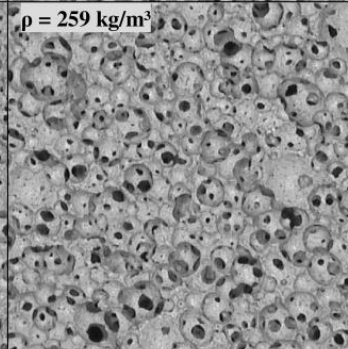
#### 4.2.3 *Porous structure*

Table 6 presents the porous structure of GFCs cured at 20°C. GFC porous structure depended strongly on both its H<sub>2</sub>O<sub>2</sub> and surfactant contents. Whatever the H<sub>2</sub>O<sub>2</sub> content, reducing the surfactant content promoted the formation of big bubbles. In the fresh state, paste was dense and contained small entrained bubbles. The amount of air entrained increased with surfactant content. O<sub>2</sub> gas-off created several large bubbles in the paste volume that could come into contact. When two bubbles came into contact, a surfactant membrane could appear between them, preventing gas exchange. The membrane could remain stable until the matrix set, or break (coalescence) if the surfactant content was not sufficient to stabilize it. When the surfactant content was small, some coalescence could occur without collapse of the GFC fresh structure because the bubbles still had an acceptable radius (samples HP<sub>1.5</sub>S<sub>0.0025</sub> and HP<sub>1.5</sub>S<sub>0.0025</sub> -

Table 6). The number of bubbles decreased and their average diameter increased. Higher surfactant content hindered coalescence and led to a finer, homogenous porous structure (surfactant content = 0.05% -

Table 6). However, the compressive strength results revealed that this type of fine structure was not associated with the highest bearing ability. Thus, low surfactant content led to controlled coalescence. It was associated with larger pores made of larger bubbles separated by wider matrix walls. Adapting the surfactant content improved GFC compressive strength for a given density. However, high surfactant content could also hinder matrix setting. These phenomena have been highlighted for calcium sulphate by Samson (2015). With geopolymer, the mechanisms leading to matrix setting are very different but an overdose of surfactant may impede the geopolymerization process. Controlling the GFC porous structure may also be very interesting for other applications such as energy storage systems (Ndiaye, Ginestet, & Cyr, 2017) or filtration (Strozi Cilla, Colombo, & Raymundo Morelli, 2014).

**Table 6. Porous structure evolution depending on H<sub>2</sub>O<sub>2</sub> and surfactant content (each picture represents 12.5<sup>2</sup> mm<sup>2</sup>).**

		H <sub>2</sub> O <sub>2</sub> content		
		1 %	1.5 %	2 %
Surfactant content	0.0025 %	 $\rho = 507 \text{ kg/m}^3$	 $\rho = 349 \text{ kg/m}^3$	Coalescence
	0.0125 %	 $\rho = 441 \text{ kg/m}^3$	 $\rho = 336 \text{ kg/m}^3$	 $\rho = 255 \text{ kg/m}^3$
	0.050 %	 $\rho = 411 \text{ kg/m}^3$	 $\rho = 314 \text{ kg/m}^3$	 $\rho = 259 \text{ kg/m}^3$

## 5 Conclusion

GFCs with good thermomechanical performances were produced. First, the best proportions of MK, FA and activator were identified. The optimized composition regarding IST, shrinkage and compressive strength was obtained with 25% of activator, 62.5% of MK and 12.5 of FA (A<sub>25</sub>MK<sub>62.5</sub>FA<sub>12.5</sub>). A small percentage of OPC was added to reduce the IST (from 380 to 290 minutes) and to reduce the time between the end of fresh GFC rising (180 minutes) and the geopolymer matrix setting.

GFCs were produced with three H<sub>2</sub>O<sub>2</sub> contents (1, 1.5 and 2 %) to control GFC densities. Three surfactant contents (0.05, 0.0125 and 0.0025%) were employed and a significant evolution of the porous structure was observed. Low densities were achieved ( $226 < \rho < 506 \text{ kg/m}^3$ ), which resulted in good thermal insulation ability ( $0.07 < \lambda < 0.12 \text{ W/(m.K)}$ ) and acceptable compressive strength ( $0.5 < R_c < 1.85 \text{ MPa}$ , for samples cured at 20°C). Reducing the surfactant content led to porous structures made of larger bubbles separated by wider matrix walls and promoted GFC compressive strength. The produced GFCs exhibit good compressive strength in comparison with the FC found on literature.

## 6 References

- ASTM C191 - 01. (2006). ASTM C191 - 01 - Standard Test Method for Time of Setting of Hydraulic Cement by Vicat Needle. ASTM.
- ASTM C596 - 09e1. (2001, September). ASTM C596 - 09e1 - Standard Test Method for Drying Shrinkage of Mortar Containing Hydraulic Cement. ASTM.
- Ducman, V., & Korat, L. (2016). Characterization of geopolymer fly-ash based foams obtained with the addition of Al powder or H<sub>2</sub>O<sub>2</sub> as foaming agents. *Materials Characterization*, 113, 207–213. <https://doi.org/10.1016/j.matchar.2016.01.019>
- Duxson, P., Fernández-Jiménez, A., Provis, J. L., Lukey, G. C., Palomo, A., & Deventer, J. S. J. van. (2006). Geopolymer technology: the current state of the art. *Journal of Materials Science*, 42(9), 2917–2933. <https://doi.org/10.1007/s10853-006-0637-z>
- Duxson, P., Provis, J. L., Lukey, G. C., & van Deventer, J. S. J. (2007). The role of inorganic polymer technology in the development of “green concrete.” *Cement and Concrete Research*, 37(12), 1590–1597. <https://doi.org/10.1016/j.cemconres.2007.08.018>

- Hlaváček, P., Šmilauer, V., Škvára, F., Kopecký, L., & Šulc, R. (2015). Inorganic foams made from alkali-activated fly ash: Mechanical, chemical and physical properties. *Journal of the European Ceramic Society*, 35(2), 703–709. <https://doi.org/10.1016/j.jeurceramsoc.2014.08.024>
- Kamseu, E., NGouloure, Z. N. M., Ali, B. N., Zekeng, S., Melo, U. C., Rossignol, S., & Leonelli, C. (2015). Cumulative pore volume, pore size distribution and phases percolation in porous inorganic polymer composites: Relation microstructure and effective thermal conductivity. *Energy and Buildings*, 88, 45–56. <https://doi.org/10.1016/j.enbuild.2014.11.066>
- Kaynakli, O. (2012). A review of the economical and optimum thermal insulation thickness for building applications. *Renewable and Sustainable Energy Reviews*, 16(1), 415–425. <https://doi.org/10.1016/j.rser.2011.08.006>
- Kutchko, B. G., & Kim, A. G. (2006). Fly ash characterization by SEM–EDS. *Fuel*, 85(17–18), 2537–2544. <https://doi.org/10.1016/j.fuel.2006.05.016>
- Lassinantti Gualtieri, M., Romagnoli, M., & Gualtieri, A. F. (2015). Preparation of phosphoric acid-based geopolymer foams using limestone as pore forming agent – Thermal properties by in situ XRPD and Rietveld refinements. *Journal of the European Ceramic Society*, 35(11), 3167–3178. <https://doi.org/10.1016/j.jeurceramsoc.2015.04.030>
- Masi, G., Rickard, W. D. A., Vickers, L., Bignozzi, M. C., & van Riessen, A. (2014). A comparison between different foaming methods for the synthesis of light weight geopolymers. *Ceramics International*, 40(9, Part A), 13891–13902. <https://doi.org/10.1016/j.ceramint.2014.05.108>
- Ndiaye, K., Ginestet, S., & Cyr, M. (2017). Modelling and experimental study of low temperature energy storage reactor using cementitious material. *Applied Thermal Engineering*, 110, 601–615. <https://doi.org/10.1016/j.applthermaleng.2016.08.157>
- Novais, R. M., Ascensão, G., Buruberri, L. H., Senff, L., & Labrincha, J. A. (2016). Influence of blowing agent on the fresh- and hardened-state properties of lightweight geopolymers. *Materials & Design*, 108, 551–559. <https://doi.org/10.1016/j.matdes.2016.07.039>
- Pacheco-Torgal, F., Abdollahnejad, Z., Camões, A. F., Jamshidi, M., & Ding, Y. (2012). Durability of alkali-activated binders: A clear advantage over Portland cement or an unproven issue? *Construction and Building Materials*, 30, 400–405. <https://doi.org/10.1016/j.conbuildmat.2011.12.017>



- Pacheco-Torgal, F., Faria, J., & Jalali, S. (2012). Embodied Energy versus Operational Energy. Showing the Shortcomings of the Energy Performance Building Directive (EPBD). *Materials Science Forum*, 730-732, 587–591. <https://doi.org/10.4028/www.scientific.net/MSF.730-732.587>
- Palmero, P., Formia, A., Antonaci, P., Brini, S., & Tulliani, J.-M. (2015). Geopolymer technology for application-oriented dense and lightened materials. Elaboration and characterization. *Ceramics International*, 41(10, Part A), 12967–12979. <https://doi.org/10.1016/j.ceramint.2015.06.140>
- Perez Fernandez, N. (2008). *The influence of construction materials on life cycle energy use and carbon dioxide emissions of medium size commercial buildings* (PhD Thesis). Victoria University, Wellington.
- Pouhet, R. (2015). *Formulation and durability of metakaolin-based geopolymers*. LMDC Toulouse, France.
- Provis, J. L., Palomo, A., & Shi, C. (2015). Advances in understanding alkali-activated materials. *Cement and Concrete Research*, 78, Part A, 110–125. <https://doi.org/10.1016/j.cemconres.2015.04.013>
- Ramamurthy, K., Kunhanandan Nambiar, E. K., & Indu Siva Ranjani, G. (2009). A classification of studies on properties of foam concrete. *Cement and Concrete Composites*, 31(6), 388–396. <https://doi.org/10.1016/j.cemconcomp.2009.04.006>
- Samson, G. (2015). *Synthèse et propriétés de mousses minérales* (PhD Thesis). INSA Rennes, LGCGM, France.
- Samson, G., Phelipot-Mardelé, A., & Lanos, C. (2016a). A review of thermomechanical properties of lightweight concrete. *Magazine of Concrete Research*, 1–16. <https://doi.org/10.1680/jmacr.16.00324>
- Samson, G., Phelipot-Mardelé, A., & Lanos, C. (2016b). Thermal and mechanical properties of gypsum–cement foam concrete: effects of surfactant. *Journal European Journal of Environmental and Civil Engineering*, 0. <https://doi.org/10.1080/19648189.2016.1177601>
- Sanjayan, J. G., Nazari, A., Chen, L., & Nguyen, G. H. (2015). Physical and mechanical properties of lightweight aerated geopolymer. *Construction and Building Materials*, 79, 236–244. <https://doi.org/10.1016/j.conbuildmat.2015.01.043>
- San Nicolas, R., Cyr, M., & Escadeillas, G. (2014). Performance-based approach to durability of concrete containing flash-calcined metakaolin as cement replacement. *Construction and Building Materials*, 55, 313–322. <https://doi.org/10.1016/j.conbuildmat.2014.01.063>
- Strozi Cilla, M., Colombo, P., & Raymundo Morelli, M. (2014). Geopolymer foams by gelcasting. *Ceramics International*, 40(4), 5723–5730. <https://doi.org/10.1016/j.ceramint.2013.11.011>

- Zhang, Z., Provis, J. L., Reid, A., & Wang, H. (2014). Geopolymer foam concrete: An emerging material for sustainable construction. *Construction and Building Materials*, *56*, 113–127. <https://doi.org/10.1016/j.conbuildmat.2014.01.081>
- Zhang, Z., Provis, J. L., Reid, A., & Wang, H. (2015). Mechanical, thermal insulation, thermal resistance and acoustic absorption properties of geopolymer foam concrete. *Cement and Concrete Composites*, *62*, 97–105. <https://doi.org/10.1016/j.cemconcomp.2015.03.013>
- Zuhua, Z., Xiao, Y., Huajun, Z., & Yue, C. (2009). Role of water in the synthesis of calcined kaolin-based geopolymer. *Applied Clay Science*, *43*(2), 218–223. <https://doi.org/10.1016/j.clay.2008.09.003>